electronics

Article

Harmonic Suppression Strategy of LCL Grid-Connected PV Inverter Based on Adaptive QPR_PC Control

Shengqing Li, Shuishuang Zhou and Huanping Li *

School of Electrical and Information Engineering, Hunan University of Technology, Zhuzhou 412007, China; zhoushuishuang@163.com (S.Z.)
* Correspondence: hpl252@outlook.com

Abstract: To reduce the influence of voltage harmonics on the grid current, a control strategy based on adaptive quasi-proportional phase compensated resonance (QPR_PC) is proposed. Firstly, the LCL grid-connected photovoltaic inverter system model is established, and the stability performance of the three-level inverter system under double closed-loop control is analyzed using the output impedance model of the inverter. Then, a QPR regulator for the zero steady-state error tracking of AC signals is studied. To solve the problem that the system has poor robustness against frequency changes when the traditional QPR regulator is used in the static coordinate system, this paper improves the traditional QPR regulator to optimize the response characteristics of the closed-loop system. Based on the QPR regulator, a phase margin compensation structure is introduced to form QPR_PC control. Then adaptive frequency design is added to ensure good control even when the power grid frequency drifts, which is the control strategy proposed in this paper. Verification shows that the proposed method improves the phase margin of output impedance at a specific frequency, restrains the interference of the 3rd, 5th, and 7th harmonics of grid voltage, and improves the dynamic performance of the system and the quality of grid-connected current. Finally, the simulation results show that the total harmonic distortion rate of grid-connected current is reduced by 1.03% after adopting this strategy, which verifies the effectiveness and correctness of the proposed method.

Keywords: PV grid-connected inverter; improved quasi-proportional resonant resonance control; phase margin compensation; no static difference tracking; harmonic suppression

Citation: Li, S.; Zhou, S.; Li, H. Harmonic Suppression Strategy of LCL Grid-Connected PV Inverter Based on Adaptive QPR_PC Control. *Electronics* **2023**, *12*, 2282. https://doi.org/10.3390/electronics12102282

Academic Editor: Ahmed F. Zobaa

Received: 6 March 2023
Revised: 29 March 2023
Accepted: 4 April 2023
Published: 18 May 2023

1. Introduction

The continuous expansion of distributed generation systems, multiple transformers, and long transmission lines is used for interconnection and connection systems [1]. Therefore, in the modern distributed generation system of the public power grid, the inverter cannot be ignored, and its structure and control strategy will directly affect the power quality of the grid [2]. In photovoltaic power generation systems, many non-linear devices are usually connected at the point of common coupling (PCC) of the grid-connected inverter to ensure living needs. After the harmonic current generated by these devices passes through the line impedance, the grid voltage at PCC contains more harmonics, eventually leading to the distortion of the grid-connected current and the instability of the power system [3,4]. Renewable energy is fed to the power grid by a grid-connected inverter, which constitutes a local microgrid. Therefore, grid-connected inverter technology is one of the key technologies for renewable energy utilization. Grid-connected inverters generally use current source control under pulse-width modulation(PWM) to inject large amounts of high-frequency current into the grid and affect the grid's quality [5,6]. To filter out the high-frequency current, a filter inductor is usually added between the inverter and the grid. Many scholars have proposed an LCL filter [7]. Compared with the traditional L-type filter, an LCL filter provides a high-frequency bypass through the capacitor branch, thus greatly attenuating the high-frequency component of the current flowing into the grid, which is widely used in high-power equipment.

The three-phase sinusoidal input is still a sinusoidal quantity in a two-phase stationary coordinate system and, therefore, cannot be controlled using a PI regulator [8]. Although static error can be reduced using PI plus power grid voltage feed-forward control, static error still cannot be completely eliminated. In addition, due to the low-frequency harmonics in the inverter output, the PI regulator cannot eliminate such harmonics [9]. Quasi-proportional resonance (QPR) control proposed in some literature can provide infinite gain at a specified frequency, thus achieving static error-free control at a specific frequency [10,11]. If the resonance control is added at 3, 5, 7, etc., harmonics of these frequencies can be eliminated in a targeted manner, and the quality of current injected into the grid can be significantly improved [12].

To improve the stability and robustness of the system to grid-connected harmonics, several control strategies for grid-connected inverters are proposed. A notch-like digital filter-based single-loop active damping method is proposed in [13] to make the LCL inverter property parameters and characteristic grid changes robust. In [14], the authors demonstrated the existing admittance coupling among multiple parallel inverters and obtained the multiple parallel grid-connected inverter's admittance by considering the influence of PLL with the admittance coupling factor. In [15], the authors studied a harmonic voltage distortion damping method to parallel-connected LCL-type inverters in islanded operations, which includes a P + Repetitive controller and the parallel virtual-admittance control. The performance of controllers with different phase compensation is analyzed and compared in [16]. This paper reveals that the traditional PI and HQR controllers with P-GVF are unsuitable for parallel applications. In the low-frequency band, the output impedance of the inverter is passivated by WP-GVF and HQR-PC controllers improved by the traditional control method. In the high-frequency band, the system has the minimum phase characteristic after using PQR-PC for delay compensation. Multiple harmonic quasi-resonant (HQR) controllers are used in [17] to suppress harmonic current. This proves that the maximum order of a plug-in HQR controller is limited by the control bandwidth, which is significantly reduced due to grid impedance. To reduce the computational number and complexity, the control parameter design method based on the dual-current loop active damping scheme is proposed in [18]. The harmonic suppression method is proposed in [19] for quasi-proportional resonant of multiple parallel inverters and voltage external trap control. Focus on a traditional inverter, an improved active damping inhibition strategy based on PIR current controller is proposed in [20], which can effectively inhibit system resonance, though this strategy makes it difficult to accurately track command current and makes no static difference in the tracking of harmonic components.

Given the limitations in the above literature, the stability analysis of output impedance under double closed-loop control and the correlation between grid-connected voltage and grid-connected current are described in detail in this paper, thus affecting the stability of an LCL grid-connected inverter cluster system. The QPR_PC current control strategy with phase compensation is adopted to improve the output impedance phase margin at a specific subfrequency and to track the AC component of a specific frequency. The influence of network voltage on network current is suppressed quickly. This scheme ensures the excellent quality of the system and improves the stability of the LCL grid-connected inverter. Finally, the effectiveness of the proposed strategy is verified by simulation and experimental analysis.

2. Mathematical Model of LCL Photovoltaic Grid-Connected Inverter

In this section, the relationship between the ratio of power grid impedance and output impedance is found after a comprehensive analysis of the output impedance model of the LCL grid-connected inverter based on double closed-loop control.

2.1. System Model

The cluster system model of LCL grid-connected photovoltaic inverters studied in this paper is shown in Figure 1, where C_1,C_2 are the support capacitors of the DC side; PVi is the photovoltaic array, where #i = 1, 2, 3, . . . ,n; three-phase state variable u_g, i_1, are grid voltage, inverter side current, grid current; $Z_g = sL_g$ is the grid perceptual impedance; L_1, L_2, C is LCL filter side inductance, network side inductance, and filter capacitor. I* is grid current [21–23].

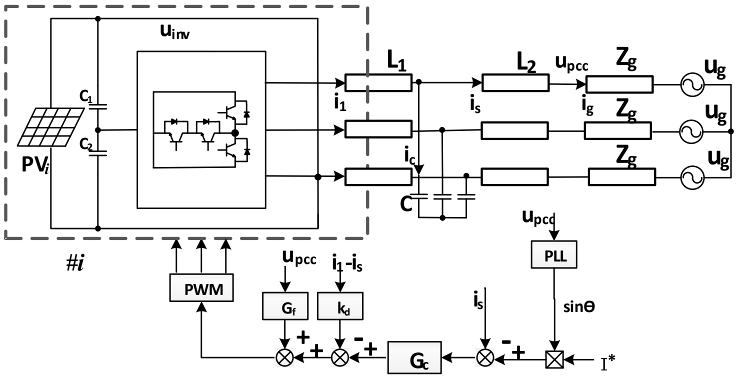

Figure 1. LCL photovoltaic parallel inverter system model.

The parasitic resistance and inductance of the filter capacitor are ignored [24]; the quantitative relationship between variables of the LCL filter in Figure 1 is:

$$\begin{cases} L_1 \frac{di_{L1}}{dt} = u_{\text{inv}} - u_c \\ C \frac{du_c}{dt} = i_L - i_s \\ L_2 \frac{di_{L2}}{dt} = u_c - u_{pcc} \end{cases} \tag{1}$$

2.2. Inverter Output Impedance Model

According to Equation (1), the equivalent model of inverter #i in the continuous domain is shown in the dotted line part in Figure 2a. Figure 2a is the application of capacitive current i_1 and grid-connected current i_{L2} feedback double closed-loop control block diagram; where kd is the active damping proportional coefficient, PWM amplification gain $k_{PWM} = 1$, i_{ref} is a grid-connected current reference value, U_{PCC} is the grid-connected point voltage, G_c is the current loop control function, and G_d is the delay function introduced in the digital control process, namely:

$$G_d(s) = \frac{1}{T_S} \frac{1 - e^{-T_s s}}{s} e^{-T_s s} \tag{2}$$

where *Ts* is the sampling and switching period.

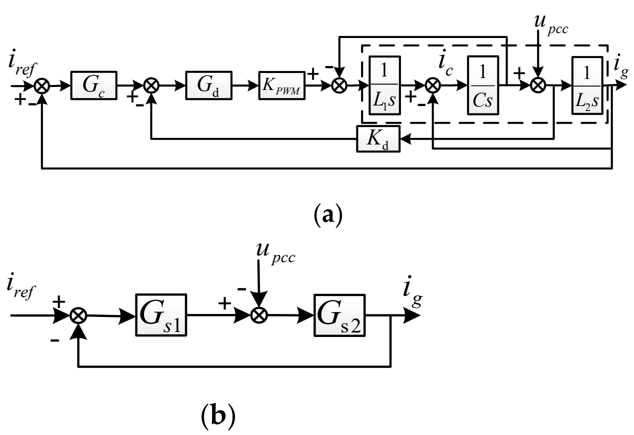

Figure 2. Control block diagram of the double closed-loop control under the s domain. (**a**) Control block diagram; (**b**) Simplified model.

The open-loop transfer function of the system is:

$$G_o = G_c k_{pwm} G_d / \left[s^3 C L_1 L_2 + s^2 k_{pwm} G_d k_d \left(L_2 + L_g \right) C + s \left(L_1 + L_2 + L_g \right) \right] \tag{3}$$

Equivalent transformation of Figure 2a yielded Figure 2b. Among them:

$$\begin{aligned} G_{s1} &= k_{pwm} G_d G_c / [1 + sCk_{pwm} k_d G_d + s^2 L_1 C] \\ G_{s2} &= [1 + sCk_{pwm} k_d G_d + s^2 L_1 C] / [s(L_1 + L_2 + L_g) \\ &\quad + s^2 (L_2 + L_g) C k_{pwm} k_d G_d + s^3 L_1 (L_2 + L_g) C] \end{aligned}$$

The mesh current i_g of the #i inverter can be derived from Figure 2b:

$$i_g = G_0 i_{ref} - Y_0 u_{pcc} \tag{4}$$

In Equation (4), G_0 is the closed-loop transfer function of the current reference value to the inverter output current:

$$G_0 = \left. \frac{i_g}{i_{ref}} \right|_{u_{pcc}=0} = \frac{G_{s1} G_{s2}}{1 + G_{s1} G_{s2}} \tag{5}$$

Y_0 is a closed-loop transmission function of the grid voltage to the inverter output current:

$$Y_0 = \left. \frac{i_g}{u_{pcc}} \right|_{i_{ref}=0} = \frac{G_{s2}}{1 + G_{s1} G_{s2}} \tag{6}$$

It can be seen as an equivalent output guide of the inverter. Then the current control inverter can be described using a Norton model; namely, the current source is parallel with the output conductor Y_0 [25]. A Norton model of the n-parallel inverter system can be built from the perspective of each sub-frequency converter, as shown in Figure 3a.

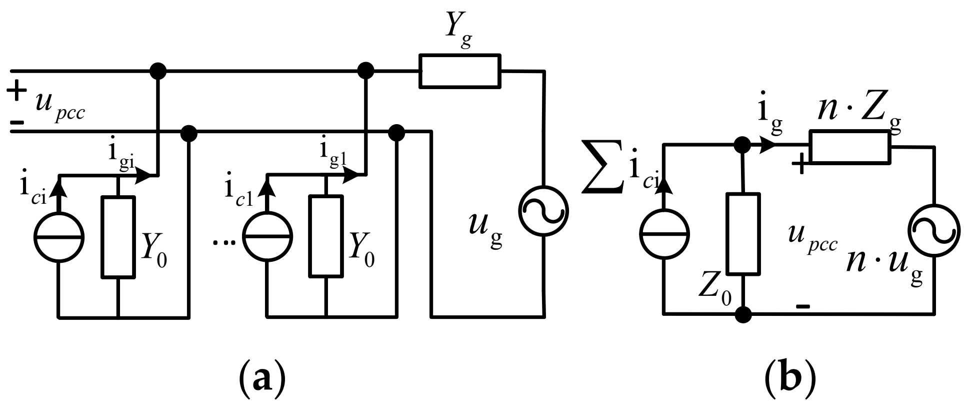

Figure 3. An impedance model considering the control effect. (**a**) The impedance model; (**b**) Simplified model.

2.3. Stability Analysis

According to Figure 3a, the line current i_{gi} of the #i inverter is known:

$$i_{\mathrm{gi}} = i_{\mathrm{ci}} - u_{pcc} Y_0 \tag{7}$$

and

$$u_{pcc} = \frac{i_{\mathrm{ci}} + \sum\limits_{\mathrm{j \neq i}}^{n} i_{\mathrm{cj}} + u_g Y_g}{n Y_0 + Y_g} \tag{8}$$

According to the literature [26,27], when all inverters have the same working conditions and the same parameters and n parallel inverters are taken as the whole, the circulating current is approximately 0. Therefore, a simplified equivalent impedance model of N parallel inverters can be established from the perspective of PCC, as shown in Figure 3b. The injection current i_{gi} of the #*i* inverter, which can be derived:

$$i_{\mathrm{gi}} = \frac{Z_0}{Z_0 + nZ_g} \sum_{\mathrm{i}=0,1\ldots}^{n} i_{\mathrm{ci}} - n\frac{u_g}{Z_0 + nZ_g} \tag{9}$$

In Equation (9), the quality of the grid current of the LCL grid-connected inverter system under double closed-loop control is related to nZ_g/Z_0 and ug. When gate impedance $Z_{\mathrm{g}} \neq 0$, in order to ensure system stability, the phase margin θ_{PM} between Z_{g} and Z_0 satisfying Nyquist criterion should be greater than zero. Therefore, the subsequent research mainly focuses on ensuring the amplitude margin and phase margin of the output impedance.

3. QPR_PC Control Strategy

3.1. The QPR Control Policy

According to the analysis in the previous section, to maintain good system stability, effective control strategies can be adopted to improve the amplitude margin and phase margin of the output impedance Z_0. The output impedance of the inverter under double closed-loop control is expressed by Equation (6):

$$\begin{aligned} Z_0 = [&k_{pwm}G_dG_c + s(L_1 + L_2 + L_g) + s^2(L_2 + L_g)Ck_{pwm}k_dG_d \\ &+ s^3L_1(L_2 + L_g)C]/[1 + sCk_{pwm}k_dG_d + s^2L_1C] \end{aligned} \tag{10}$$

In (10), the amplitude margin and phase margin of output impedance Z_0 can be adjusted by designing the current controller G_c. The *QPR* regulator is widely used due to its good performance and low cost in a static coordinate system for fundamental wave AC tracking. Therefore, this section mainly analyzes the performance of the *QPR* regulator applied in double closed-loop knowable conditions.

The typical *QPR* controller transfer function expression is:

$$G_{QPR} = k_p + \frac{2k_r\omega_c s}{s^2 + 2\omega_c s + {\omega_0}^2} \tag{11}$$

where k_p is the proportional gain and k_r is the resonant gain; ω_0 = $2\pi f_0$ is base wave angular frequency; ω_c is resonance term bandwidth, which increasing ω_c can improve the adaptability of *QPR* controller to power grid voltage frequency.

The gain at ω_0 is:

$$G_{QPR}(j\omega_0) = \sqrt{{k_p}^2 + (\frac{k_r\omega_c\omega_0}{{\omega_0}^2 + \omega_c\omega_0})^2} \tag{12}$$

According to (12), the *QPR* controller has infinite gain at ω0 to realize AC signal control without static error and small steady-state error. The Bode diagram corresponding to the PR controller is shown in Figure 4. It can be seen that the gain of the proportional resonance controller does tend to infinity at the set resonant frequency. If the control system in Figure 4 adopts the *QPR* controller, the closed-loop transfer function of the system tends to 1 at the resonant frequency; that is, the input reference signal is tracked theoretically without error. However, without improvement, the *QPR* controller inevitably has its defects; that is, when the grid voltage frequency deviates from the fundamental frequency, the *QPR* in the mains frequency controller gain falls sharply, no longer going to infinity, so that the tracking grid voltage frequency sine to time unable to realize zero steady-state error, and the resulting system control effect is poor. If the parameters *kp* and *kr* are set improperly, the controller gain at the reference signal frequency becomes negative. The controller will suppress the reference signal instead, which deteriorates the control performance of the whole system. Therefore, the influence of the voltage and frequency fluctuation of the power grid on the controller must be considered.

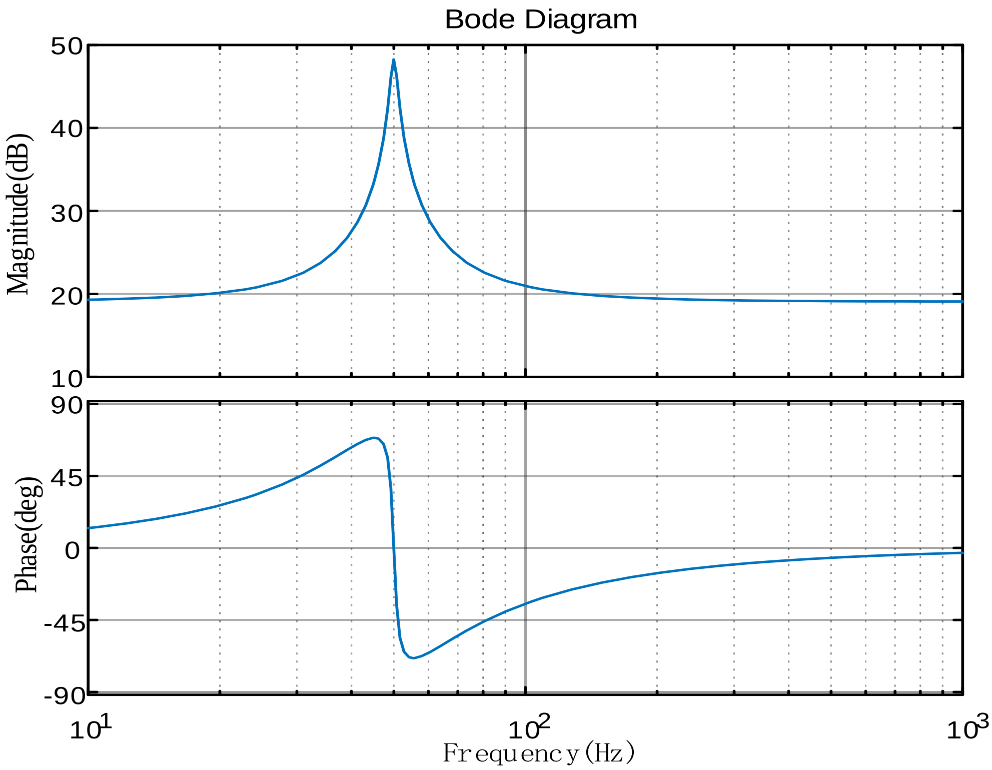

Figure 4. The Bode diagram corresponding to the PR controller.

In the industrial field, the frequency of commercial power often fluctuates, especially in harsh environments of electricity consumption, such as a local weak power grid system on the edge of the edge power grid, a system powered by a diesel generator, an independent wind power system, or places where electricity is in short supply. When the frequency fluctuation, the control effect of the resonance controller will be affected, especially the resonance controller working at three, five, and seven times of fundamental wave frequency resonance point, the influence is very obvious. Therefore, to effectively improve the anti-power grid frequency disturbance ability of the PR controller, reduce its sensitivity to power grid frequency fluctuation so that it can still maintain a good control effect when the power grid frequency drift has a strong practical guiding significance.

3.2. QPR_PC Control Strategy

To solve the problem of a system subject to frequency changes when the traditional QPR regulator is used in the static coordinate system, this paper improves the traditional QPR regulator to optimize the response characteristics of the closed-loop system. To effectively suppress harmonic components at a specific frequency and enable the current controller to output high-quality power grid current even under power grid voltage disturbance, a QPR regulator with phase compensation is proposed, as shown in Figure 5. Compared to the traditional QPR regulator, the QPR_PC regulator maintains the high-gain characteristic in the fundamental frequency, not only processing the current reference signal through the proportion compensation and harmonic compensation but also adding the phase margin compensation, which improves the performance of the grid current tracking under the grid voltage disturbance.

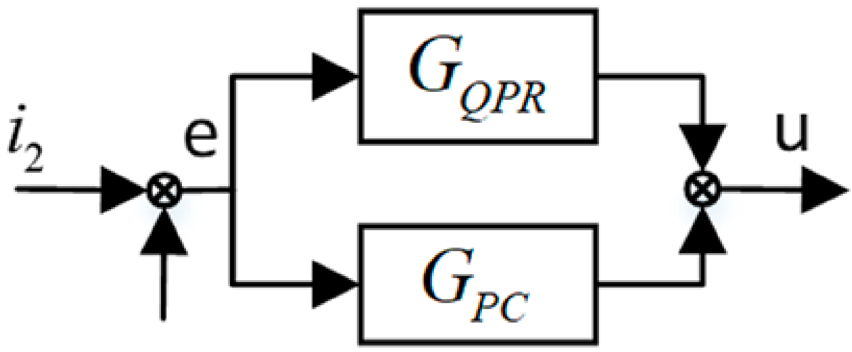

Figure 5. Structural block diagram with harmonic phase compensation added.

As shown in Figure 4, the *QPR* expression at the base frequency is:

$$G_{QPR} = k_p + k_r \frac{\omega_c s}{s^2 + \omega_c s + {\omega_0}^2} \tag{13}$$

The phase margin compensation expression at a particular harmonic frequency is:

$$G_{PC} = \sum_{n=3,5,7} k_r \frac{\sqrt{1-\lambda_n^2}s - n\lambda_n\omega_0}{s^2 + 2\omega_c s + (n\omega_0)^2} \tag{14}$$

In Equation (14), the relationship between the phase angle lag quantity θ_n, λ_n, and θ_n to determine the harmonic frequency is:

$$\theta_n = \arctan(\lambda_n / \sqrt{1-{\lambda_n}^2}) \tag{15}$$

In the actual system operation process, the system parameters will change with the change of external factors, which will have an important impact on the system's performance, especially the LCL filter parameters. Due to the increase in temperature and current, the inductance, capacitance, and resistance values will change greatly. Therefore, it is necessary to analyze the influence of filter parameters on the closed-loop poles of the system to ensure the robustness of the system during operation. The LCL filter and system parameters obtained in this paper are shown in Table 1.

Table 1. Paramenters of the grid-connected inverters system.

Parameter	Numerical Value
DC bus voltage, U_{dc}	800 V
Power rating, P	5 kW
Inverter side inductance, L_1	0.78 mH
Net side electrical feeling, L_2	0.45 mH
Filter capacitor, C	6.8 µF
Power grid voltage, U_g	220 V
Frequency of sampling, f_s	15 kHz
Resonance frequency, f_c	1 kHz
Power grid voltage frequency, f	50 Hz

According to the principle of control theory, to make the system stable, the system's roots must be distributed in the left half plane of the coordinate system. Secondly, the system parameters should be designed with a certain margin so that the system can still work stably when the parameters of the LCL filter change. Thirdly, to ensure that the system can effectively suppress the resonant link of the LCL filter and improve the quality of the output current, the poles generated by the LCL filter should have enough damping to attenuate the oscillation, and should be kept away from the virtual axis to weaken the influence on the system. Since the QPR controller only affects its resonant frequency, at the system crossover frequency ω_i, the G_c can be approximately equal to the k_p, binding Table 1 parameters available:

$$k_p = 2\pi(L_1 + L_2 + L_g) f_c \tag{16}$$

In this paper, k_p is set to 9.2. The harmonic suppression structure with the 3rd, 5th, and 7th harmonics phase compensation is shown in Figure 5.

The resonance bandwidth ω_c = $2\pi f_c$ = 6.3. For the system to have sufficient gain at $n\omega_0$, it should satisfy:

$$20\lg\left(\frac{k_r}{\omega_c}\right) > 40dB \tag{17}$$

Here, the k_r value is 600.

The ideal phase angle θ_n* between the modified QPR controller and λ_n is:

$$\lambda_n = \frac{\omega_c k_p \tan\theta_n^* + \sqrt{k_r^2 \tan^2\theta_n^* - (\omega_c k_p \tan\theta_n^*)^2 + k_r^2}}{k_r(1 + \tan^2\theta_n^*)} \tag{18}$$

To stabilize the system under the control of the QPR_PC above $-45°$at $n\omega_0$, λ_3 = 0.454, λ_5 = 0.643, and λ_7 = 0.666 are selected; the parameters of the QPR_PC controller are shown in the table below.

The bode diagram corresponding to the QPR controller can be drawn from Table 2 parameters, combining Equations (11), (13) and (14).

Table 2. The QPR_PC controller parameters.

Parameter	Numerical Value
Proportional gain, k_p	9.2
Harmonic gain, k_r	600
Tuning bandwidth, ω_c	6.3
λ_3	0.454
λ_5	0.643
λ_7	0.766

Figure 6 shows the bode diagram corresponding to the QPR controller. It can be seen that the QPR_PC controller does not change the general trend of the original QPR controller; that is, it maintains the original stability margin and turn frequency. Compared with the latter, the system can maintain a larger gain at a specific frequency, $n\omega_0$, and effectively suppress the influence of power grid voltage disturbance on the system. This solves the problem of the poor robustness of the system against frequency changes when using the traditional QPR regulator in a static coordinate system to optimize the response characteristics of the closed-loop system. It provides a large gain for the system to realize the station-free tracking of the ac component with the frequency $n\omega_0$. At the same time, according to the control theory, the larger the open-loop gain of the system, the stronger the ability to resist the disturbance in the ring. Therefore, the system has a strong resistance to the interference of the $n\omega_0$ frequency.

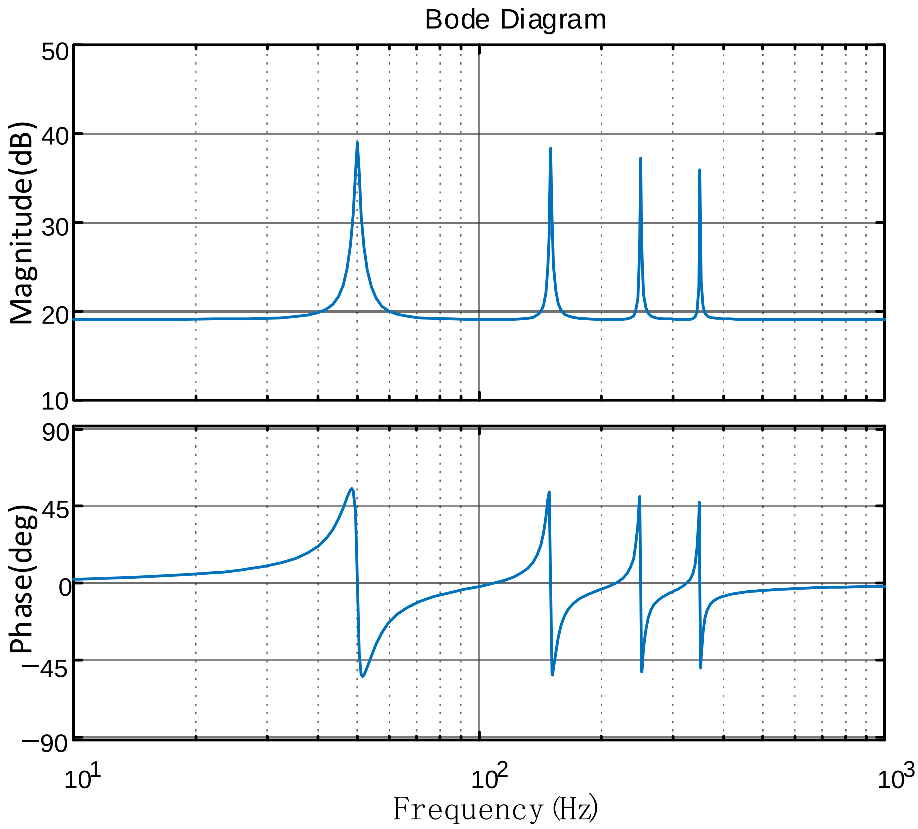

Figure 6. The bode diagram corresponding to the QPR controller.

According to Equations (11), (13) and (14) and combining the parameters of Tables 1 and 2, a Potter diagram of the output impedance Z_0 under QPR control and QPR_PC control is shown in Figure 7.

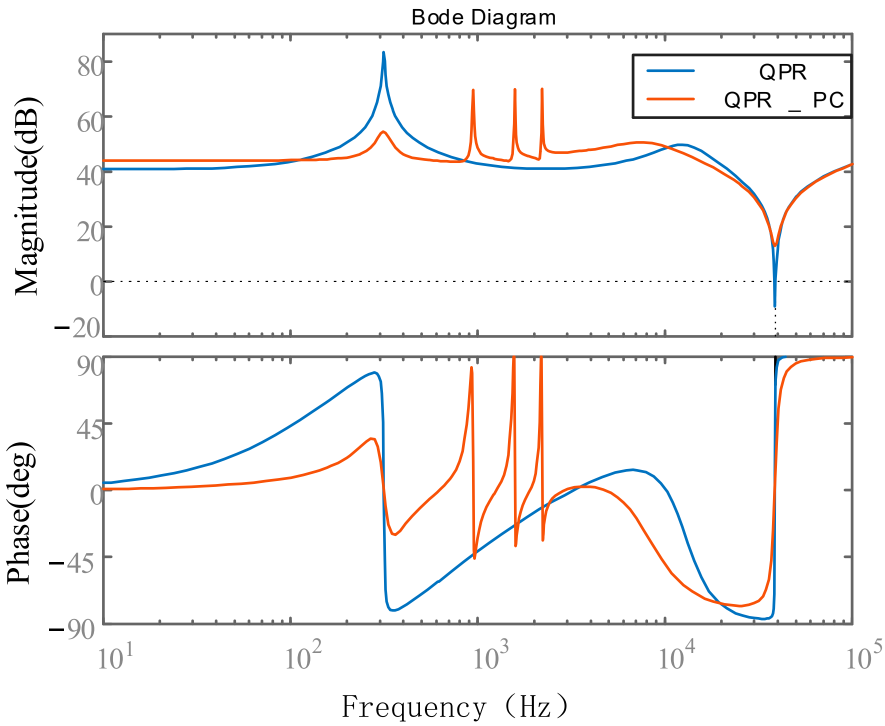

Figure 7. Output impedance Z_0 Potter diagram.

Figure 7 illustrates the output impedance Z_0 under the control of QPR. Obviously, it has an amplitude of high modulus over 40 dB in the low-frequency band, which favors the suppression of the harmonic. However, the phase of Z_0 is similar to the $-90°$ line, requiring more inverters in parallel, which may lead to system instability. In contrast, the QPR_PC control proposed in this paper can not only keep the output impedance Z_0 at high amplitude but also improve the phase margin of Z_0, in particular at specific frequencies, due to the addition of the phase margin compensation link; the harmonic of the power grid is well suppressed, effectively improving the system's stability.

In conclusion, the QPR_PC control strategy of band phase margin compensation proposed in this paper can not only reduce system cost but also track the base wave component of the grid current under the condition of grid voltage disturbance, effectively inhibit the main low harmonic, improve the quality of grid-connected current, and then improve the stability of the grid-connected system. The poor robustness of the system against the frequency change is solved when the traditional QPR regulator is used in the static coordinate system, and the response characteristics of the closed-loop system are optimized.

3.3. Adaptive Frequency Design

The cutoff frequency ω_c is mainly used to restrain the power grid frequency fluctuation and the adverse influence of the precision limit on the control effect in the digital realization of the transfer function. The value of ω_c does not affect the gain of the QPR controller at the resonant frequency $n\omega_0$. When the power grid frequency fluctuation is small, ω_c can be taken to a smaller value, and the frequency signal in a smaller bandwidth range can have a high enough steady-state gain by adjusting k_r. However, the allowable frequency deviation of China's power grid for small-capacity systems is ± 0.5 Hz, and the harmonic frequency fluctuation range is an integer multiple of this. When the ω_c value is small, the actual harmonic frequency can be outside the high-gain band range of the controller, so it is difficult to achieve zero steady-state error control of the harmonic signal.

By increasing the cutoff frequency ω_c or resonant control gain k_r, the gain of the control system in the frequency fluctuation range can be improved, but the system's stability will be reduced.

In the actual operation, the power grid frequency does not fluctuate dramatically, and the harmonic frequency is always an integer multiple of the fundamental frequency. To realize the robust adaptive of the control system to the frequency fluctuation, a digital phase-locked loop (DPLL) is adopted in this paper to detect the power frequency period $T_0(=1/f_0)$ of the system in real-time, and the analog-to-digital conversion chip is controlled to make the sampling number N in unit power frequency period T_0 fixed. In this case, the sampling period $T_s = 1/(Nf_0)$, Zn can be expressed as:

$$Z_n = \frac{n\omega_0}{\tan(n\pi/N)} \tag{19}$$

According to Equation (19), the corresponding difference equation of the QPR controller with harmonic number n is:

$$y_n(k) = k_r Y_n(u_n(k) - u_n(k-2)) - X_{1n} y_n(k-1) X_{2n} y_n(k-2) \tag{20}$$

where $y_n(k)$ is the output of the QPR controller with harmonic number n; $u_n(k)$ is the input to the corresponding QPR controller. And:

$$Y_n = \frac{2\omega_c Z_n}{{Z_n}^2 + 2\omega_c Z_n + {\omega_n}^2} \tag{21}$$

In Equation (21), n is the given harmonic number, n is a constant, and the fluctuation of system frequency leads to the change of ω_c/ω_0 value. Since the value of ω_c only affects the controller's bandwidth, allowing a certain adjustment range, and the fluctuation of power grid frequency during actual operation is small, ω_c/ω_0 can be set as a constant.

$$k = \left.\frac{\omega_c}{\omega_0}\right|_{\omega_0 = 2\pi f_e} \tag{22}$$

where f_e is the rated frequency of the power grid, and f_e = 50 Hz. $n\omega_0$ is always based on the resonant frequency point of the difference Equation (20) of the QPR controller with this coefficient, thus ensuring the robustness of the control system against frequency fluctuation. In the specific implementation, W_C only needs to restrain the adverse influence of precision limitation in the digital implementation of the transfer function on the control effect, so the constant k should be a smaller value.

The Potter diagram of output impedance Z_0 based on adaptive QPR_PC control is shown in Figure 8. It can be seen from the figure that the application of adaptive QPR_PC control can greatly improve the amplitude and phase of output impedance Z_0, improve the anti-interference of the system, and ensure the stability of the system. Because the resonant angular frequency is very stable, even during the process of power grid voltage distortion or mutation, adaptive QPR_PC resonance output can remain stable. The integral output fluctuations in the power grid voltage mutation moment, though not completely, is a dc component. The rotation transformation will generate a harmonic under the static coordinate system and reduce the system's stability. The adaptive QPR_PC controller has stronger power grid adaptability. The harmonic output content of adaptive QPR_PC is very small, so the output current waveform is very sinusoidal.

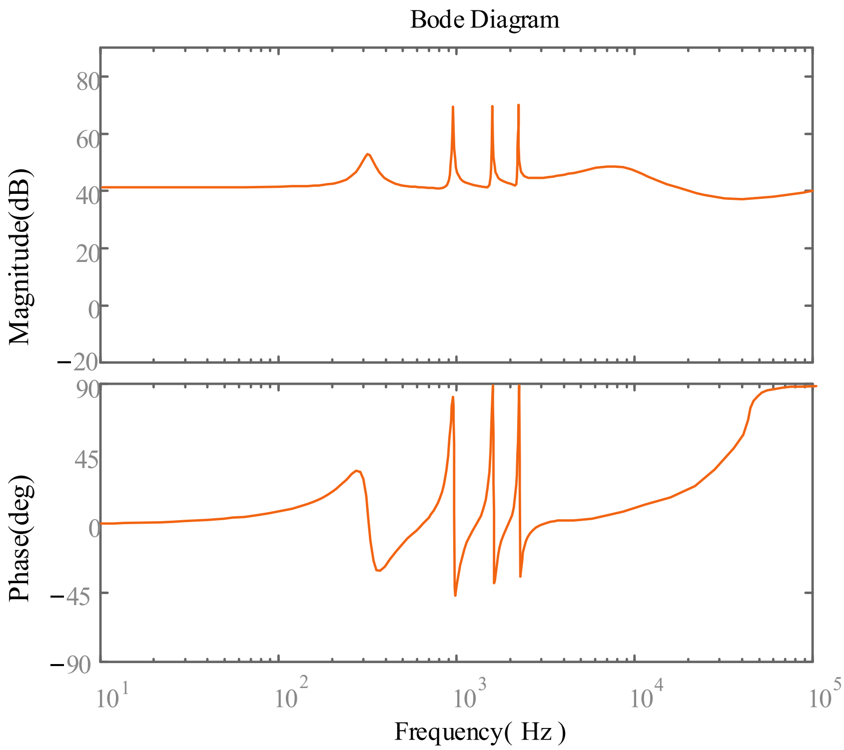

Figure 8. Potter diagram of output impedance Z_0 based on adaptive QPR_PC control.

To reduce the burden on the QPR regulator, voltage feed-forward upcc is also introduced into the system control, as shown in Figure 1. The voltage feed-forward upcc is directly proportional to the grid voltage and inversely proportional to the DC side voltage. The modulation wave is output by the feed-forward quantity upcc and the current loop PR regulator. Feed-forward reduces the burden of the PR regulator in the modulation process, so the adjustment speed of DC bus fluctuation can be improved, and its response speed can be increased by adding feed-forward.

Where G_f is the proportional feed-forward coefficient of power grid voltage, and when G_d is ignored, the angular frequency of the denominator D_{Z0} is:

$$f_{cor} = \frac{1}{2\pi}\sqrt{\frac{1-G_f}{L_1 C}} \tag{23}$$

To avoid a 90° phase lag caused by G_f = 1, thus affecting the passive characteristics of Z_0, the f_{cor} is pushed away from the inverter bandwidth f_{bw} to alleviate the phase delay. According to Equation (23), the following equation can be obtained:

$$G_f < 1 - L_1 C(2\pi f_{bw})^2 \tag{24}$$

When G_f = 0.7, it can guarantee type (8) was set up without significantly reduced $|Z_0|$, improving the stability of the low-frequency band. This section may be divided by subheadings. It should provide a concise and precise description of the experimental results, their interpretation, as well as the experimental conclusions that can be drawn.

4. Simulation and Experimental Verification

4.1. Incisive

To verify the effectiveness of the proposed method, the type T three-level grid-connected inverter model was built in the simulation software Matlab/Simulink for analysis, and the parameters are shown in Tables 1 and 2. The PV power side voltage Udc and the grid voltage Ug are provided by the DC constant voltage source and the AC voltage source, respectively, in which the Ug contains the 3rd, 5th, and 7th harmonics; the grid impedance Zg is simulated by a series of inductance between the PCC point and the Ug.

Figure 9a,b are the reference current i_{ref} and grid current i_g waveforms during QPR control and adaptive QPR_PC control strategy. We can see that the grid-connected current contains many of the 3rd, 5th, and 7th harmonics and the phase lag. Under the adaptive QPR_PC control, the grid current can also track the reference current excellently, and the current quality is significantly improved.

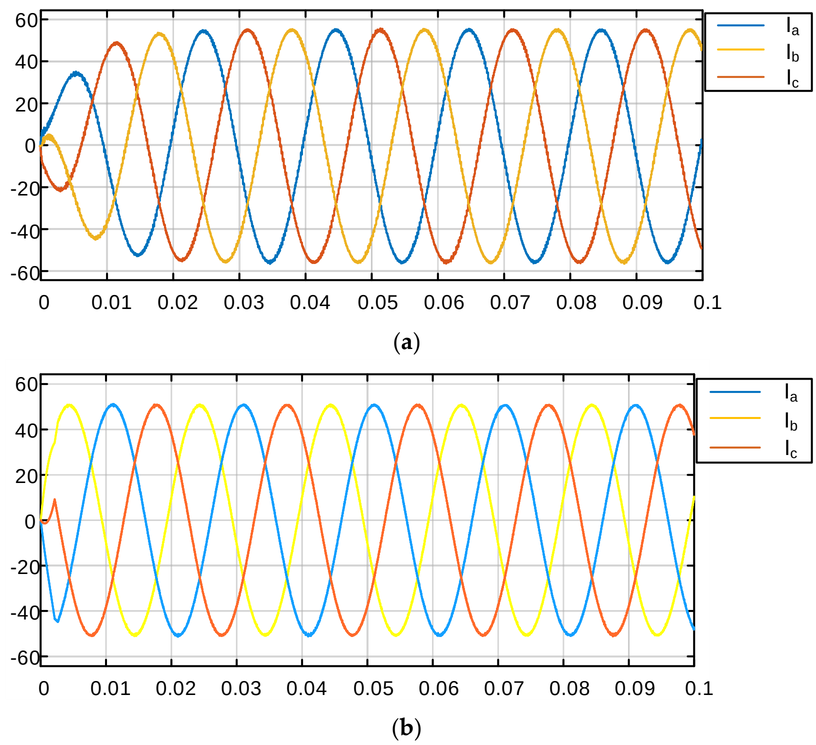

Figure 9. Simulation waveform of the grid-connected inverter. (**a**) QPR control; (**b**) QPR_PC control.

Figure 10 shows the parallel current THD analysis using the QPR control strategy and the adaptive QPR_PC control strategy proposed. The harmonic distortion rate of the grid-connected current has changed from 1.97% to 0.94%, reduced by 1.03%, which shows that the control strategy can effectively reduce the grid-connected current harmonic, improve the current quality, and verify the effectiveness of the control strategy proposed in this paper.

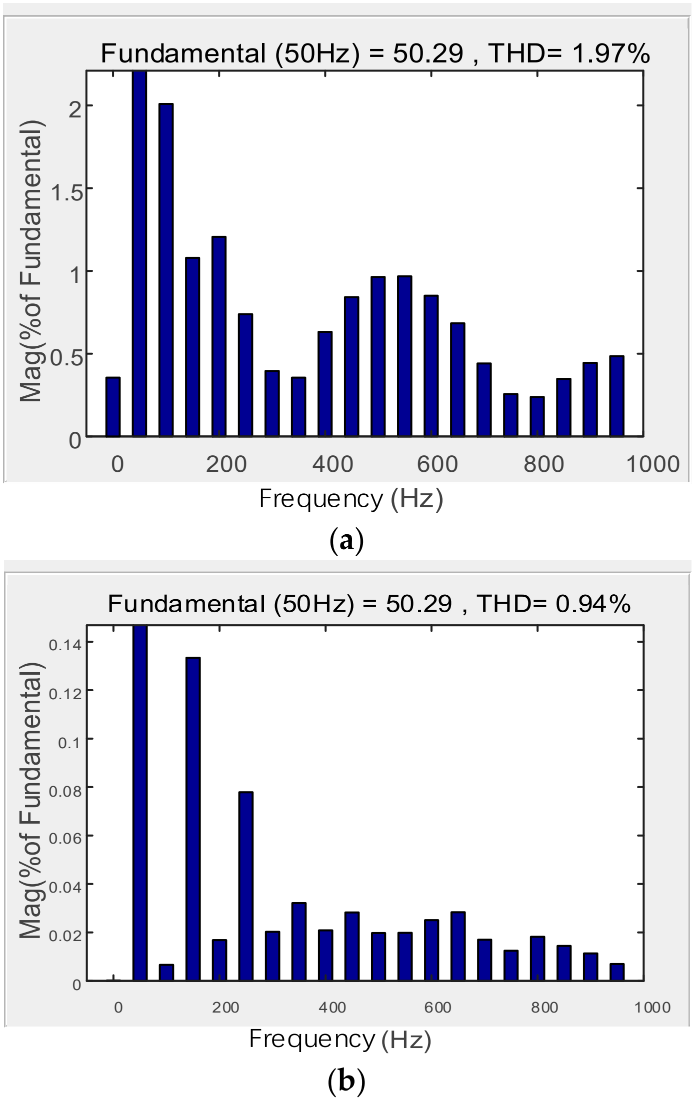

Figure 10. Grid-connected current THD. (**a**) QPR control; (**b**) QPR_PC control.

From the simulation results, the proposed control strategy can effectively reduce the grid-connected current harmonic and improve the current quality.

4.2. Validation

To verify the effectiveness of the control strategy of a three-phase LCL grid-connected inverter, a three-phase LCL grid-connected inverter is built in this paper for experiments. The parameters of the experimental platform are the same as those in the previous table. In the experiment, a programmable AC source is used to simulate the distorted network conditions. Figure 11 shows the experimental waveform of grid-connected current under the traditional grid voltage feed-forward control and the proposed coordinated control strategy.

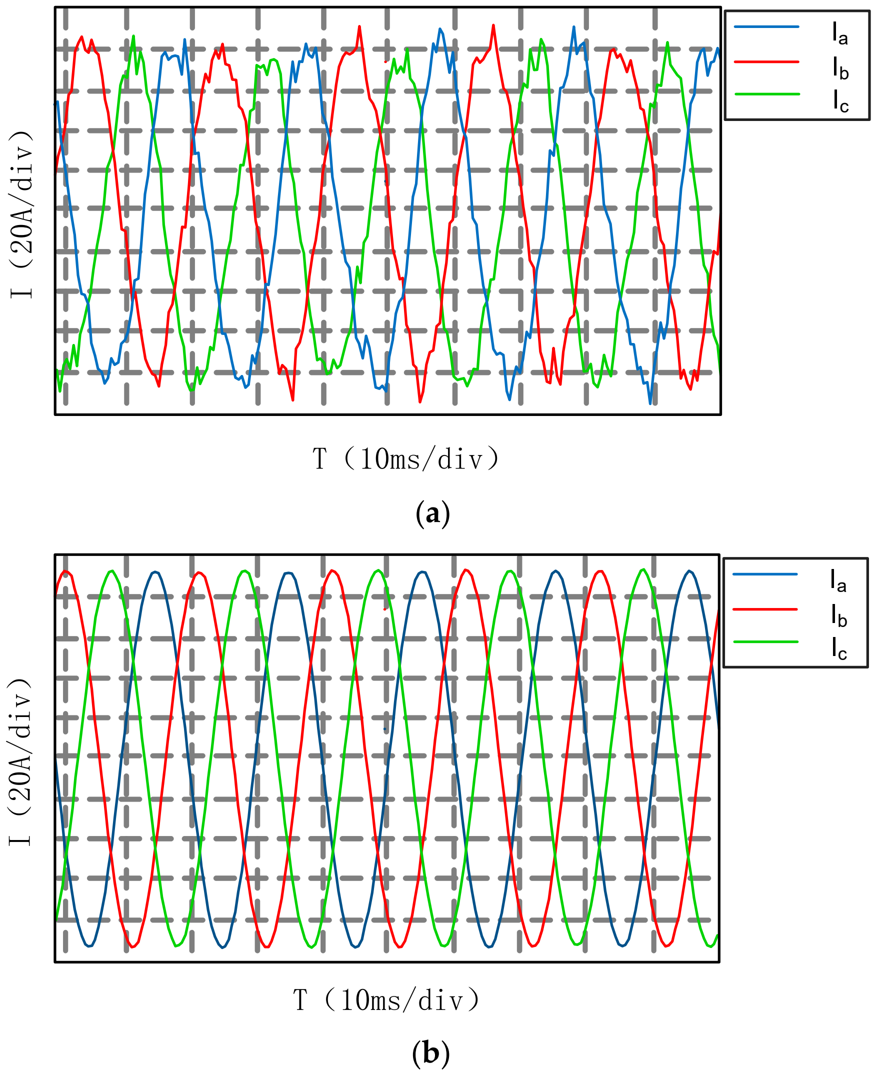

Figure 11. Experimental waveform. (**a**) Traditional power grid voltage feed-forward control; (**b**) The proposed coordination control.

By comparing Figure 11a,b, it can be seen that the current is seriously distorted when the traditional power grid voltage feed-forward control is adopted, while the current is perfect when the proposed coordinated control strategy is adopted. Therefore, it can be seen that the proposed coordinated control strategy can effectively suppress the harmonic content, ensure the system's stability, and improve the power quality, which verifies the conclusions mentioned above.

5. Conclusions

In LCL grid-connected photovoltaic inverter systems, the factors affecting stability include grid-connected impedance and grid-connected voltage. To improve the stability of the grid-connected inverter, a control strategy based on adaptive QPR_PC was proposed in a static coordinate system to solve the problem of multi-frequency component interference during compensation, and phase margin compensation was introduced based on QPR control. Simulation results show that compared with classical QPR control, the proposed control strategy can effectively suppress the adverse effects of the system and effectively track the current without any difference. Through simulation and experimental verification, the harmonic distortion rate of the connection current is reduced by 1.03%, and the waveform of the grid-connected current has better quality, indicating that the system can resist the interference of the 3rd, 5th, and 7th harmonics. LCL grid-connected inverter cluster system runs stably and can inject high-quality current. There are still some theoretical and practical problems in the study of this manuscript. Experiments based on four parallel grid-connected inverters further verify the effectiveness of the proposed control method.

Author Contributions: Conceptualization, S.L., S.Z. and H.L.; methodology, S.Z. and H.L.; formal analysis, S.Z.; writing—original draft preparation, S.Z. All authors have read and agreed to the published version of the manuscript.

Funding: This research was funded by National Natural Science Fund, grant number 51977072.

Institutional Review Board Statement: Not applicable.

Informed Consent Statement: Not applicable.

Data Availability Statement: Not applicable.

Conflicts of Interest: The authors declare no conflict of interest.

References

1. Sun, P.; Yao, J.; Liu, R.; Pei, J.; Zhang, H.; Liu, Y. Virtual Capacitance Control for Improving Dynamic Stability of the DFIG-Based Wind Turbines During a Symmetrical Fault in a Weak AC Grid. *IEEE Trans. Ind. Electron.* **2021**, *68*, 333–346. [CrossRef]
2. Xu, S.; Shao, R.; Cao, B.; Chang, L. Single-phase grid-connected PV system with golden section search-based MPPT algorithm. *Chin. J. Electr. Eng.* **2021**, *7*, 25–36. [CrossRef]
3. Muhammad, S.; Hanif, A.K.K.M. Robust L Approximation of an LCL Filter Type Grid-Connected Inverter Using Active Disturbance Rejection Control under Grid Impedance Uncertainty. *Energies* **2021**, *14*, 064104.
4. Zhou, L.; Guerrero, J.M.; Zhou, X.; Chen, Y.; Lv, Z.; He, Z.; Wu, W.; Yang, L.; Yan, K.; Luo, A. Inverter-Current-Feedback Resonance-Suppression Method for LCL-Type DG System to Reduce Resonance-Frequency Offset and Grid-Inductance Effect. *IEEE Trans. Ind. Electron.* **2018**, *65*, 7036–7048. [CrossRef]
5. Gabour, N.E.H.; Habbi, F.; Bounekhla, M.; Boudissa, E.G. Enhanced Harmonic Elimination Using Genetic Algorithm Optimization in Multilevel Inverters. In Proceedings of the 2021 18th International Multi-Conference on Systems, Signals & Devices (SSD), Monastir, Tunisia, 22–25 March 2021; pp. 323–329.
6. Alawieh, H.; Tehrani, K.A.; Azzouz, Y.; Dakyo, B. A new active common-mode voltage elimination method for three-Level Neutral-Point Clamped inverters. In Proceedings of the IECON 2014-40th Annual Conference of the IEEE Industrial Electronics Society, Dallas, TX, USA, 29 October–1 November 2014; pp. 1060–1066.
7. Jiang, S.; Liu, Y.; Liang, W.; Peng, J.; Jiang, H. Active EMI Filter Design with a Modified LCL-LC Filter for Single-Phase Grid-Connected Inverter in Vehicle-to-Grid Application. *IEEE Trans. Veh. Technol.* **2019**, *68*, 10639–10650. [CrossRef]
8. Yao, W.; Yang, Y.; Zhang, X.; Blaabjerg, F.; Loh, P.C. Design and Analysis of Robust Active Damping for LCL Filters Using Digital Notch Filters. *IEEE Trans. Power Electron.* **2017**, *32*, 2360–2375. [CrossRef]
9. Xie, B.; Guo, K.; Mao, M.; Zhou, L.; Liu, T.; Zhang, Q.; Hao, G. Analysis and Improved Design of Phase Compensated Proportional Resonant Controllers for Grid-Connected Inverters in Weak Grid. *IEEE Trans. Energy Convers.* **2020**, *35*, 1453–1464. [CrossRef]
10. Xie, Z.; Chen, Y.; Wu, W.; Wang, Y.; Gong, W.; Guerrero, J. Frequency Coupling Admittance Modeling of Quasi-PR Controlled Inverter and Its Stability Comparative Analysis Under the Weak Grid. *IEEE Access* **2021**, *9*, 94912–94922. [CrossRef]
11. Wang, R.; Wang, S.; Gong, Z.; Li, M.; Zhang, Y.; Huang, M. Design of Single-phase Photovoltaic Inverter Based on Double Closed-loop PI and Quasi-PR Control. In Proceedings of the 2020 IEEE 2nd International Conference on Architecture, Construction, Environment and Hydraulics (ICACEH), Hsinchu, Taiwan, 25–27 December 2020; pp. 80–82.
12. Dong, H.; Yuan, S.; Han, Z.; Ding, X.; Ma, S.; Han, X. A comprehensive strategy for power quality improvement of multi-inverter-based microgrid with mixed loads. *IEEE Access* **2018**, *6*, 30903–30916. [CrossRef]
13. Cai, P.; Wu, X.; Yang, Y.; Yao, W.; Liu, W.; Blaabjerg, F. Design of Digital Filter-based Highly Robust Active Damping for LCL-filtered Grid-tied Inverters. In Proceedings of the 2018 IEEE 4th Southern Power Electronics Conference (SPEC), Singapore, 10–13 December 2018; pp. 1–8.
14. Zhou, W.; Torres-Olguin, R.E.; Wang, Y.; Chen, Z. A Gray-Box Hierarchical Oscillatory Instability Source Identification Method of Multiple-Inverter-Fed Power Systems. *IEEE J. Emerg. Sel. Top. Power Electron.* **2021**, *9*, 3095–3113. [CrossRef]
15. Zhou, L.; Wu, W.; Chen, Y.; Jiang, J.; Zhou, X.; Yang, L.; He, Z.; Yan, K.; Luo, A. Harmonic Voltage Distortion Damping Method for Parallel-Connected LCL-Type Inverters in Islanded Operation. *IEEE Trans. Ind. Electron.* **2019**, *66*, 9032–9044. [CrossRef]
16. Ni, Z.; Qian, Q.; Xie, S.; Xu, J.; Zeng, B. Harmonic Suppression and Stability Enhancement for Grid-Connected Inverters Based on UPQC. In Proceedings of the 2018 IEEE Energy Conversion Congress and Exposition (ECCE), Portland, OR, USA, 23–27 September 2018; pp. 4922–4926.
17. Shen, G.; Zhu, X.; Zhang, J.; Xu, D. A new feedback method for PR current control of LCL-Filter-Based Grid-Connected inverter. *IEEE Trans. Ind. Electron.* **2010**, *6*, 2033–2040. [CrossRef]
18. Xin, Z.; Mattavelli, P.; Yao, W.; Yang, Y.; Blaabjerg, F.; Loh, P. Mitigation of grid-current distortion for LCL-filtered voltage-source inverter with inverter-current feedback control. *IEEE Trans. Power Electron.* **2018**, *33*, 6248–6261. [CrossRef]

19. Ronnberg, S.K.; Gil-De-Castro, A.; Medina-Gracia, R. Supraharmonics in European and north American low-voltage networks. *IEEE Commer. Power Syst.* **2018**, 1–6.
20. Xu, J.; Qian, Q.; Zhang, B.; Xie, S. Harmonics and Stability Analysis of Single-Phase Grid-Connected Inverters in Distributed Power Generation Systems Considering Phase-Locked Loop Impact. *IEEE Trans. Sustain. Energy* **2019**, *10*, 1470–1480. [CrossRef]
21. Wang, Y.; Wang, X.; Blaabjerg, F.; Chen, Z. Harmonic Instability Assessment Using State-Space Modeling and Participation Analysis in Inverter-Fed Power Systems. *IEEE Trans. Ind. Electron.* **2017**, *64*, 806–816. [CrossRef]
22. Lu, M.; Wang, X.; Loh, P.; Blaabjerg, F. Resonance interaction of Multi-Parallel Grid-Connected inverters with LCL filter. *IEEE Trans. Power Electron.* **2017**, *32*, 894–899. [CrossRef]
23. Yu, C.; Xu, H.; Liu, C.; Wang, Q.; Zhang, X. Modeling and Analysis of Common-Mode Resonance in Multi-Parallel PV String Inverters. *IEEE Trans. Energy Convers.* **2019**, *34*, 446–454. [CrossRef]
24. Zhang, X.; Tianyi, W.; Wang, X.; Wang, G.; Chen, Z.; Xu, D. A coordinate control strategy for circulating current suppression in Multi-Paralleled Three-Phase inverters. *IEEE Trans. Ind. Electron.* **2017**, *64*, 838–847. [CrossRef]
25. Komurcugil, H.; Altin, N.; Ozdemir, S.; Sefa, I. Lyapunov-Function and Proportional-Resonant-Based Control Strategy for Single-Phase Grid-Connected VSI With LCL Filter. *IEEE Trans. Ind. Electron.* **2016**, *63*, 2838–2849. [CrossRef]
26. Lu, M.; Yang, Y.; Johnson, B.; Blaabjerg, F. An Interaction-Admittance Model for Multi-Inverter Grid-Connected Systems. *IEEE Trans. Power Electron.* **2019**, *34*, 7542–7557. [CrossRef]
27. Liang, Z.; Lin, X.; Qiao, X.; Kang, Y.; Gao, B. A Coordinated Strategy Providing Zero-Sequence Circulating Current Suppression and Neutral-Point Potential Balancing in Two Parallel Three-Level Converters. *IEEE J. Emerg. Sel. Top. Power Electron.* **2018**, *6*, 363–376. [CrossRef]